

# Research on RCS Data Validation Based on SPWVD

Jiaxin Shi<sup>1</sup>, Jun Hu<sup>2</sup>, Zhiwei Gao<sup>3,\*</sup>, Lizhong Song<sup>1</sup>,  
Huapeng Zhao<sup>2</sup>, Ran Zhao<sup>2</sup>, Wei Chen<sup>4</sup>, and Min Zhang<sup>1,4</sup>

<sup>1</sup>*School of Information Science and Engineering, Harbin Institute of Technology at Weihai, Weihai, China*

<sup>2</sup>*University of Electronic Science and Technology of China, Chengdu, China*

<sup>3</sup>*School of Information Science and Technology, Shijiazhuang Tiedao University, Shijiazhuang, China*

<sup>4</sup>*National Key Laboratory of Air-based Information Perception and Fusion, China*

**ABSTRACT:** At present, Feature Selective Validation (FSV) is the most common data verification method of computational electromagnetics, and its effectiveness has been verified since its release in 2006, but since the main research object of this method is electromagnetic compatibility data, the 8 sets of data used for algorithm training also come from the field of electromagnetic compatibility, and its data curve has the characteristics of gentle waveform and small fluctuations. However, Radar Cross Section (RCS) data, especially high-frequency RCS data, usually have complex waveforms and drastic fluctuations, and the results obtained by the FSV method are often quite different from those obtained by experts. This paper proposes a new data verification method based on Smoothed Pseudo Wigner-Ville Distribution (SPWVD) algorithm for RCS data, which integrates the characteristics of RCS data and expert evaluation experience, and verifies its effectiveness in RCS data verification.

## 1. INTRODUCTION

Radar cross section (RCS) data of objects is an important research object in the field of electromagnetics, which is the data basis for radar detection and recognition, object stealth and anti-stealth research, and plays an extremely important role in the field of national defense [1]. At present, the acquisition of RCS data is mainly based on computer simulation and experimental measurement, and on the basis of obtaining RCS data, it is necessary to use data verification technology to verify the RCS data to achieve the purpose of effective application. By comparing the consistency between simulation data and measurement data, the validity of the data, model, or method is verified, and then the correction of the simulation model or the optimization of measurement methods can be guided [2]. With the development of the times, there are higher and higher requirements for the accuracy of RCS data, and RCS data verification technology has also received extensive attention from many experts and scholars.

At present, most of the trusted verification of RCS data still relies on the visual evaluation of experts, but the subjectivity and instability of expert experience cannot realize the quantification of verification results, and this method cannot be widely applied. With the wide application of VV&A (Verification, Validation and Accreditation) method in electromagnetic credible verification, many typical statistical methods have been applied by experts and scholars to RCS data verification, such as mean square error and correlation coefficient, and are mostly used for credible verification of target results of various missiles, aircraft, ships, etc. For example, Ref. [3] uses the mean square error to verify the credibility of the RCS simulation data obtained

by different electromagnetic calculation methods, and the results show that the method is simple and easy to implement, but the results only reflect the overall error level, lack the ability to accurately locate the data differences, and cannot guide the correction of the details of the simulation model. Ref. [4] uses the Feature Selection Verification Method (FSV) to verify the credibility of the RCS data of the missile. The results show that compared with methods such as mean square error, the proposed method has greatly improved the ability of accurate positioning of differences, but there is still a big difference between the proposed method and the expert visual evaluation, which cannot meet the practical application. The reason is that the method uses the Fourier transform, which inevitably produces the problem of time-frequency resolution difference, that is, the impact of a sudden change in the data at a certain point in the time domain will be distributed to the entire frequency domain. Therefore, the current research and application of FSV is still mainly focused on the field of electromagnetic compatibility. For example, the FSV method was used in [5] to evaluate the results of the antenna's far-field pattern to verify the performance of the FSV. In [6], the FSV method was used to compare the infrared thermal images of the aircraft obtained by measurement and modeling, so as to improve the confidence of the complementarity of the measurement and modeling results. Compared with statistical methods and expert experience, the FSV method has obvious advantages in quickly locating data differences and quantitatively reflecting data characteristics. Because the main research object at the beginning of the method is electromagnetic compatibility data [2, 7, 8], the eight sets of data used for algorithm training also originate from the field of electromagnetic compatibility, and the data curve has the characteristics of gentle waveform and small fluctuations.

\* Corresponding author: Zhiwei Gao (gao\_zhiwei@163.com; gaozw@stdu.edu.cn).

**TABLE 1.** Filter weights in the frequency domain.

Frequency sequence number	Low-frequency weighted value	High-frequency weighted value
$\leq i_{bp} - 3$	1	0
$i_{bp} - 2$	0.834	0.167
$i_{bp} - 1$	0.667	0.334
$i_{bp}$	0.5	0.5
$i_{bp} + 1$	0.334	0.667
$i_{bp} + 2$	0.167	0.834
$\geq i_{bp} + 3$	0	1

However, RCS data, especially high-frequency RCS data, usually have complex waveforms and drastic fluctuations, and the results obtained by using the FSV method are often quite different from those evaluated by experts. In this paper, a data verification method based on the smoothing pseudo-Wigner-Ville distribution algorithm [9] is proposed for RCS data, which integrates the characteristics of RCS data and expert evaluation experience to improve the validity of the method for RCS data.

The structure of this paper is as follows. Firstly, the basic principles and processing flow of the FSV method are introduced in Section 2, and the limitations of the method on RCS data are analyzed through an expert investigation of 8 sets of typical RCS data. Based on the above questions, Section 3 proposes a trusted verification method for RCS data. Subsequently, Section 4 provides an example of the above method. Finally, Section 5 summarizes the full text.

## 2. INTRODUCTION TO THE FSV METHOD

This method was first proposed by Martin in 1999 [10], and after 10 years of continuous revision and improvement, it finally became the core content of the IEEE1597.1 computational electromagnetics modeling and simulation verification standard in 2008 [2]. The evaluation results of the FSV method not only reflect the numerical differences, but also contain the understanding of the differences by experts in the field, which can be used as a point-by-point analysis and overall measurement tool for data validation, and provide qualitative and quantitative evaluation indicators.

### 2.1. Flow of the FSV Method

FSV is a method of assessing the credibility of data based on its characteristics. The calculation of the difference between the two sets of data is carried out point-to-point, and the amplitude and trend are verified from many aspects. Combined with the FSV evaluation scale, the validation results were qualitatively and quantitatively evaluated. The basic principle of the FSV method is to ensure that the two sets of data have the same number of sampling points, and the data are transformed by Fourier transform to obtain the frequency domain form. The first four points in the spectrum are inversely transformed by Fourier transform, and the data obtained is the DC component. From the fifth point, the remaining data are filtered according to the unique low-pass and high-pass filters in the FSV method, and then the inverse Fourier transform is car-

ried out to obtain the low-frequency and high-frequency components respectively. The combination of DC, low-frequency, and high-frequency components forms the data difference, and then combined with the FSV evaluation grade table to obtain the evaluation grade.

#### 2.1.1. Extraction of DC, Low-Frequency, and High-Frequency Components

##### 1. Extract the DC Component

First, there are two sets of data with  $N$  points, and  $n$  is the number of data points. The frequency domain data are obtained by Fourier transform on the two sets of comparison data, and the four points with the lowest frequency in the frequency domain data are inversely transformed by Fourier transform to obtain the DC component  $DC_1(n)$  and  $DC_2(n)$ .

##### 2. Extract Low-frequency and High-frequency Components

The frequency domain data are summed from the fifth term:

$$S = \sum_{i=5}^N TDWS(i) \quad (1)$$

where  $TDWS(i)$  is the  $i$  spectral value,  $S$  the sum of spectral values starting from the fifth frequency point, and  $N$  the total number of points. The demarcation point between high and low frequencies is determined by the following formula:

$$\sum_{i=5}^{i_{40\%}} TDWS(i) \geq 0.4 \times S \quad (2)$$

$$i_{bp} = i_{40\%} + 5 \quad (3)$$

where  $i_{40\%}$  is the frequency point corresponding to 40% of the sum of the spectral values starting from the fifth frequency, and  $i_{bp}$  is the dividing point between high and low frequencies.

Then, the data are filtered according to the frequency domain filter defined by the FSV method to obtain the low-frequency and high-frequency components in the frequency domain, respectively, and then the inverse Fourier transform is performed to obtain the low-frequency components  $L_1(n)$ ,  $L_2(n)$  and high-frequency components  $H_1(n)$ ,  $H_2(n)$ , respectively. The specific low-pass and high-pass filters are shown in Table 1.

#### 2.1.2. Obtain Difference Measure

##### 1. Amplitude Difference Measure (ADM)

The amplitude difference of the ADM measurement data is mainly obtained by the combination of DC and low-frequency components, so it reflects the DC difference of the data and reflects the overall consistency. ODM is the difference of DC offset, and the formula is as follows:

$$ADM(n) = \left| \frac{\alpha(n)}{\beta} \right| + ODM \quad (4)$$

$$\alpha(n) = (|L_1(n)| - |L_2(n)|) \quad (5)$$

$$\beta = \frac{1}{N} \sum_{n=1}^N (|L_1(n)| + |L_2(n)|) \quad (6)$$

$$ODM(n) = \left| \frac{\chi(n)}{\delta} \right| \exp \left\{ \left| \frac{\chi(n)}{\delta} \right| \right\} \quad (7)$$

$$\chi = (|DC_1(n)| - |DC_2(n)|) \quad (8)$$

$$\delta = \frac{1}{N} \sum_{n=1}^N (|DC_1(n) + L_1(n)| + |DC_2(n) + L_2(n)|) \quad (9)$$

## 2. Feature Difference Measure (FDM)

FDM reflects the trend difference of the data, which is mainly obtained by the combination of derivatives of the low-frequency and high-frequency components, so it reflects the trend difference of the data. FDM1 is composed of the first derivative of the low-frequency components of the two sets of data, which reflects the difference in the slow change of the trend of the two sets of data. FDM2 is composed of the first derivative of the high-frequency components of the two sets of data, which reflects the difference in the instantaneous trend of the two sets of data. FDM3 is composed of the second derivative of the high-frequency components of the two sets of data, reflecting the more detailed trend difference between the two sets of data. Due to the existence of a second-order “derivative”, the number of data points for FDM is 4 points less than that for the original data.

$$FDM_1(n) = \frac{|L'_1(n)| - |L'_2(n)|}{\frac{2}{N} \sum_{n=1}^N (|L'_1(n)| + |L'_2(n)|)} \quad (10)$$

$$FDM_2(n) = \frac{|H'_1(n)| - |H'_2(n)|}{\frac{6}{N} \sum_{n=1}^N (|H'_1(n)| + |H'_2(n)|)} \quad (11)$$

$$FDM_3(n) = \frac{|H''_1(n)| - |H''_2(n)|}{\frac{7.2}{N} \sum_{n=1}^N (|H''_1(n)| + |H''_2(n)|)} \quad (12)$$

$$FDM(n) = 2 (|FDM_1(n) + FDM_2(n) + FDM_3(n)|) \quad (13)$$

where  $L'_{1,2}(n)$  is the first derivative of  $L_{1,2}(n)$ ;  $H'_{1,2}(n)$  is the first derivative of  $H_{1,2}(n)$ ;  $H''_{1,2}(n)$  is the second derivative of  $H_{1,2}(n)$ .

## 3. Global Difference Measure (GDM)

GDM is the global difference obtained by considering ADM and FDM comprehensively, reflecting the comprehensive difference of amplitude and change trend, and the formula is as follows:

$$GDM(n) = \sqrt{(ADM(n)^2 + FDM(n)^2)} \quad (14)$$

The GDM assessment is obtained by calculating the average of the GDM, which is denoted as the confidence assessment value.

$$GDM_c = \frac{\sum_{n=1}^N GDM(n)}{N} \quad (15)$$

As can be seen from the above,  $ADM(n)$ ,  $FDM(n)$ , and  $GDM(n)$  are point-to-point calculation of data differences, and the calculated values are based on the FSV evaluation scale to obtain qualitative and quantitative evaluation results. Table 2 shows the FSV assessment classification table.

**TABLE 2.** FSV assessment scale.

FSV value	FSV interpretation	rank
Less than 0.1	Excellent	1
Between 0.1 and 0.2	Very Good	2
Between 0.2 and 0.4	Good	3
Between 0.4 and 0.8	Fair	4
Between 0.8 and 1.6	Poor	5
Greater than 1.6	Very Poor	6

## 2.2. Analysis of the Limitations of the FSV Method in the Validation of Target RCS Data

Due to the good application effect of the FSV method applied to electromagnetic compatibility data, many scholars have tried to introduce FSV into RCS data verification. However, the applicability of the FSV method to the RCS data is limited due to the significant differences between the RCS data and EMC data.

### 2.2.1. Expert Survey for RCS Data

The FSV method is a method designed to simulate the visual evaluation of experts, so it is necessary to verify the applicability of the FSV method to the data of a particular domain by comparing it with the visual evaluation results of experts in the field. Expert results were obtained primarily through questionnaires of typical RCS data [11]. The questionnaire selected 8 sets of data as shown in Figure 1 and provided them to the respondents, which basically covered the frequencies and data characteristics commonly used at present. The survey subjects are more than 20 experts and researchers in the field of electromagnetic simulation algorithms and radar who participated in the 2024 PIERS International Conference. Respondents were asked to select six qualitative explanations in Table 1 [12] to describe the degree of similarity of each set of curves. The selected quantities of the six interpretations were counted, and

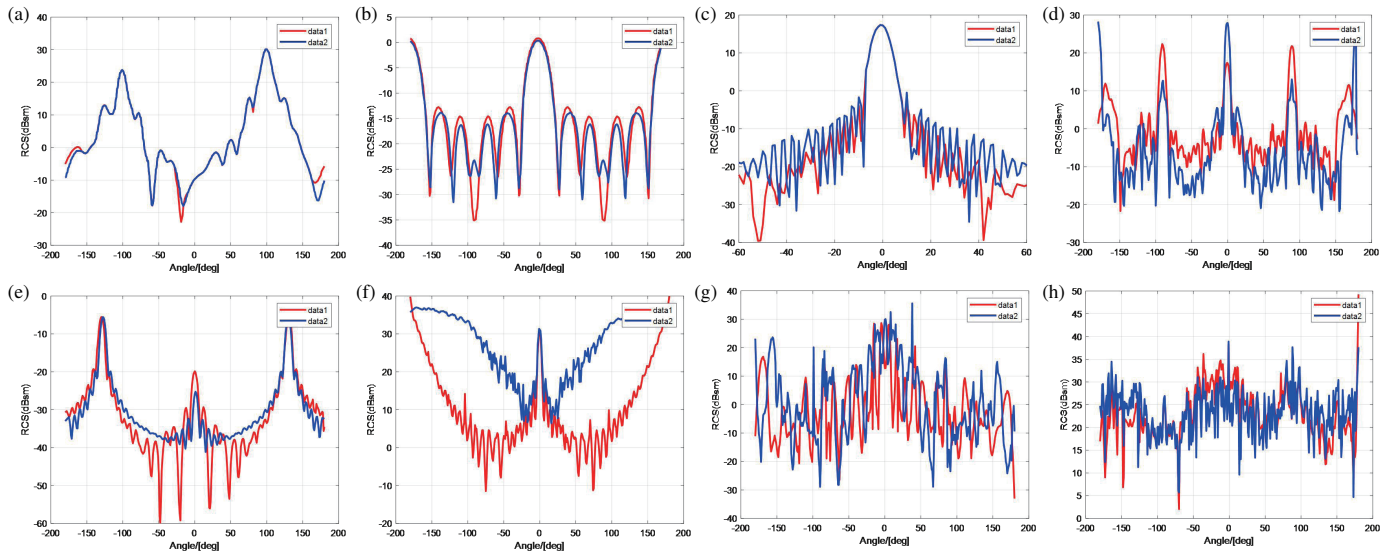


**FIGURE 1.** Questionnaire data set RCS-1 to RCS-8. (a) Data sets RCS-1. (b) Data sets RCS-2. (c) Data sets RCS-3. (d) Data sets RCS-4. (e) Data sets RCS-5. (f) Data sets RCS-6. (g) Data sets RCS-7. (h) Data sets RCS-8.

the outliers were eliminated according to the Layda criterion. In order to compare the quantitative results with the quantitative results of different methods, it is also necessary to convert the histogram results obtained by the expert survey into quantitative results, which is achieved by Equation (15).

$$GDM_{totExpert} = \sum_{i=1}^6 C_{Typical}(i) * GDM_{Expert}(i) \quad (16)$$

where  $GDM_{totExpert}$  is the quantitative result of an expert survey, in the form of a single value;  $GDM_{Expert}(i)$  is the result of the six boxes of histograms surveyed by experts, with a total of six element values, corresponding to the proportional values of the qualitative evaluation of “excellent”, “very good”, “good”, “fair”, “poor”, and “very poor”;  $C_{Typical}(i)$  is the grade value corresponding to the qualitative evaluation, as shown in Table 2,  $C_{Typical}(i) = [1 \ 2 \ 3 \ 4 \ 5 \ 6]$ .

### 2.2.2. Analysis of the Limitations of FSV in RCS Data Validation

In order to compare the evaluation performance of different methods, the evaluation results of each algorithm (including the results of expert surveys) are standardized. Observing the graph, it can be seen that data set 1 and data set 6 represent the two extremes of data differences (“excellent” and “very poor”), respectively, so the normalization of the values evaluated by different algorithms can be handled using the min-max algorithm shown in equation (17).

$$d_s(i) = \frac{d(i) - d_{\min}}{d_{\max} - d_{\min}} \quad (17)$$

where  $d(i)$  is the result of the evaluation of the differences in the data of group  $i$ ;  $d_s(i)$  is the standardized evaluation result;  $d_{\max}$  is the maximum value among the 8 groups of data evaluation

results;  $d_{\min}$  is the minimum value among the 8 groups of data evaluation results.

After standardization, the evaluation value of the data group with the largest difference in the evaluation results of each algorithm is 1, and the evaluation value of the data group with the least difference is 0. After treatment by Eq. (15) and Eq. (16), the comparison between FSV and the results of the expert survey is shown in Table 3. From the ranking results, it can be seen that the applicability of the FSV method to RCS data has great limitations. The reason is that the characteristics of EMC data are usually prominent, with obvious peaks and gentle regions, and the high and low frequency boundaries of the data are obvious.

FSV extracts the DC, low-frequency, and high-frequency components of the data based on energy to characterize the magnitude, trend, and characteristic information of the data. However, the target RCS data usually has a large number of intermediate frequency components, and the energy proportions of low, medium, and high frequencies show different characteristics with the change of radar band, and the higher the radar band is, the greater the high-frequency energy of the data is. Therefore, the energy division of FSV usually does not accurately extract the above three types of information.

In addition, the Fourier transform in the FSV algorithm cannot invert the frequency domain to the time domain position, so that the sudden change at any point on the time axis will affect the signal in the full frequency domain [13, 14], which ultimately leads to the bias between the evaluation results of the FSV algorithm and the expert evaluation results. Although many researchers have improved the failure problem by dividing the data into different regions and assigning different weights to each region or data segmentation algorithms, these methods are evaluated from the perspective of simulated experts and do not fundamentally solve the problem of bias between the evaluation results and the expert evaluation results

**TABLE 3.** Standardized evaluation results and comparison of different evaluation methods.

	Expert survey results	Expert survey sorting	FSV results	FSV sorting
Data 1	0	1	0	1
Data 2	0.4775	3	0.1407	2
Data 3	0.5020	4	0.5885	5
Data 4	0.6148	6	0.8213	7
Data 5	0.5902	5	0.4553	3
Data 6	1.0000	8	1.0000	8
Data 7	0.6373	7	0.7405	6
Data 8	0.4098	2	0.5095	4

caused by the lack of time domain localization function of the FSV algorithm.

At the same time, unlike the focus in the field of electromagnetic compatibility, in many radar applications, experts tend to pay more attention to the overall degree of agreement of the RCS data in terms of magnitude, trend, characteristics, etc., and ignore the differences in the data in terms of low RCS values and background noise and small angle offsets. However, when the FSV method is applied for data validation, these visually inattentive data may have a significant impact on the evaluation results, resulting in a large gap between the FSV and expert evaluation results.

### 3. TRUSTED VERIFICATION METHOD FOR RCS DATA

In view of the limitations of the FSV method on RCS data, this paper proposes a data trustworthiness verification method based on the Smoothed Pseudo Wigner-Ville Distribution (SPWVD) algorithm [15]. This method does not need to extract DC, low-frequency, and high-frequency components, but evaluates the data from the perspective of time-frequency energy distribution, which avoids the adverse impact of the fixed energy extraction method in FSV on the evaluation results caused by the inapplicability of RCS data. In addition, the time-frequency resolution of the Fourier transform in FSV is very low, and a sudden change at any point in the timeline will affect the signal in the full frequency domain, while SPWVD has a high time-frequency resolution [16], which can fix the influence of the difference at one point and only at that point, and do not affect the evaluation results at other points. At the same time, according to the questionnaire and experimental results, the RCS data were divided into high RCS and low RCS regions, and different evaluation weights were assigned to make them more consistent with the visual evaluation results of experts.

#### 3.1. SPWVD Algorithm

The time-frequency analysis method is a signal processing method that combines time and frequency, which can intuitively process and analyze non-stationary signals. Among them, Wigner-Ville distribution is the most typical nonlinear time-frequency analysis method, which has good time-frequency aggregation characteristics [17].

The Wigner-Ville distribution of discrete signals  $z(n)$  is defined as:

$$W_z(n, k) = \sum_{m=-N}^{m=N} z\left(n + \frac{m}{2}\right) z^*\left(n - \frac{m}{2}\right) e^{-j2\pi km/N} \quad (18)$$

Since the time-bandwidth product of the Wigner-Ville distribution reaches the lower bound given by the uncertainty principle, the time-frequency resolution of no time-frequency joint distribution can surpass the Wigner-Ville distribution.

However, when the time-frequency analysis of  $z(n)$  is performed, there is cross-term interference. Therefore, it is easy to generate false frequencies in practical application, resulting in poor final analysis results. In order to obtain good time-frequency aggregation and avoid cross-term interference, the smoothed pseudo-Wigner-Ville distribution (SPWVD) further uses two window functions to smooth the time domain and frequency domain of WVD respectively, which greatly suppresses the cross-term and ensures high time-frequency aggregation characteristics.

$$W_z^{SP}(nk) = \sum_{m=-N}^{m=N} g(n)h(k)z\left(n + \frac{m}{2}\right) z^*\left(n - \frac{m}{2}\right) e^{-j2\pi km/N} \quad (19)$$

where  $g(n)$  is the window function that suppresses the intersection of the time domain direction;  $h(k)$  is the window function that suppresses the intersection of the direction of the frequency domain.

#### 3.2. SPWVD-ON-RCS Algorithm

The basic idea of this method is shown in Figure 2. First, the data are offset level corrected to ensure that the two signals do not cross between zeros. Then, the minimum threshold of the RCS core region of interest is calculated, and the difference between the maximum and minimum of the data is  $\frac{3}{4}$ . In this paper, a weight of 0.75 is assigned to the core areas of interest [11]. For the RCS value that is less than the threshold of the core area of interest, its influence on the overall evaluation results should be weakened, so a weight of 0.25 is assigned to it. Next, the SPWVD transformation is performed on the two sets

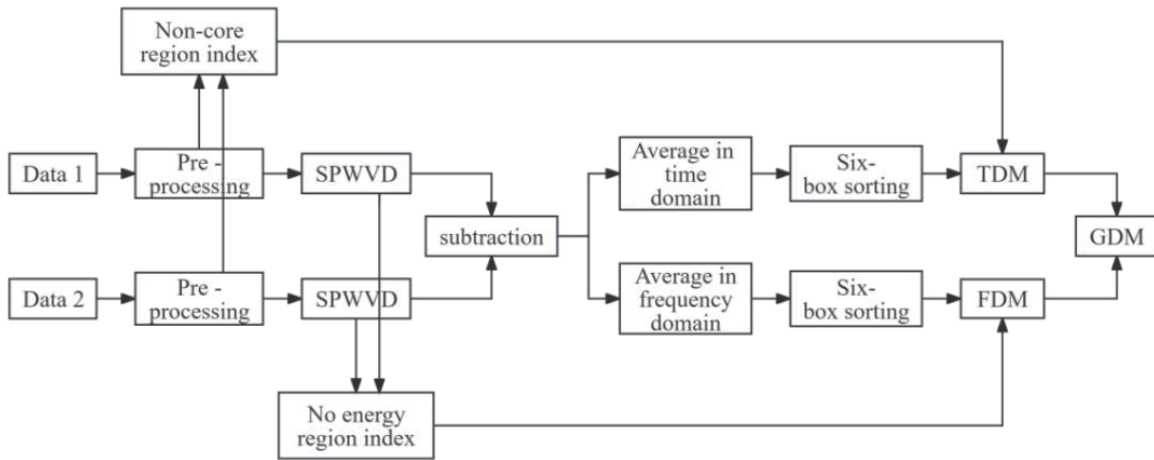


FIGURE 2. SPWVD-ON-RCS algorithmic flow.

of data. After the transformation, the time-frequency energy distribution map of the two sets of data is obtained, and then it is normalized to prevent the influence of different data magnitudes. At the same time, the frequency points without energy distribution in the frequency dimension of the two arrays were counted separately to prevent the influence of the non-energy distribution area on the evaluation results. Then, the difference between the two time-frequency energy distribution maps is obtained, and the mean values of the corresponding columns are obtained according to the time domain and frequency domain, respectively. Then, the calculation results were classified point by point according to Table 4, and the influence of non-core area and non-energy distribution area on the evaluation results was considered separately. The evaluation results in the time domain and frequency domain were obtained, respectively. Finally, the global evaluation results are obtained. The following is the detailed process of the algorithm and the corresponding formula.

TABLE 4. Classification evaluation table for six boxes.

SPWVD-ON-RCS value	SPWVD-ON-RCS interpretation	rank
Less than 0.0025	Excellent	1
Between 0.0025 and 0.05	Very Good	2
Between 0.05 and 0.1	Good	3
Between 0.1 and 0.15	Fair	4
Between 0.15 and 0.2	Poor	5
Greater than 0.2	Very Poor	6

1. Offset level correction: Prevent the adverse effects of data crossing [11].

$$Data_i(n) = Data_i(n) + DC_{cor} \quad (20)$$

where  $Data_i(n)$  is all the points of the two sets of data,  $i = 1, 2$ , and  $DC_{cor}$  is the maximum absolute value of the two sets of data.

2. Calculate the minimum threshold for the core area of interest of the RCS: In the visual evaluation of experts, experts tend to pay more attention to the region with high RCS values, and low RCS values are tolerable to a certain extent, even if there is an error. In this paper,  $\frac{3}{4}$  of the difference between the maximum and minimum values of the data is taken as the minimum threshold for the core area of interest. See Eq. (19) and Figure 3.

$$y_{threshold} = y_{max} - \frac{3}{4}(y_{max} - y_{min}) \quad (21)$$

where  $y_{threshold}$  is the lowest threshold of the RCS core region of interest;  $y_{max}$  is the maximum value between  $Data_1$  and  $Data_2$ ;  $y_{min}$  is the minimum value between  $Data_1$  and  $Data_2$ .

3. Determine the index of points in the non-core area of interest: Step 3 divides the core area of interest and the non-core area of interest, in order to simulate the experts' attention to the core area of interest, in the final evaluation process, the core area of concern is given a weight of 0.75, and the non-core area of concern is given a weight of 0.25. A necessary step in this process is to identify the index of non-core areas of interest to ensure the accuracy of the subsequent empowerment process. The process of determining the index is shown in Eq. (20) and Figure 6.

$$x_{index} = x_{index}^{Data1} |_{y \leq y_{threshold}} \cap x_{index}^{Data2} |_{y \leq y_{threshold}} \quad (22)$$

where  $x_{index}$  is the index of the final non-core region of interest;  $x_{index}^{Data1}$  is the index of the non-core area of interest of  $Data_1$ ;  $x_{index}^{Data2}$  is the index of the non-core area of interest of  $Data_2$ ;  $x_{y \leq y_{threshold}}$  is the point in the data that is less than the threshold of  $y_{threshold}$ .

As shown in Figure 4, the reason for the intersection is that in region 1, both  $Data_1$  and  $Data_2$  are smaller than the threshold, so the index here can be used as the index for the final non-core region of interest, because the two sets of data exhibit the same unconcerned characteristics. However, in region 2,  $Data_1$  is less than the threshold, but  $Data_2$  is greater than the threshold, and in this case, the index of the region cannot be used as the

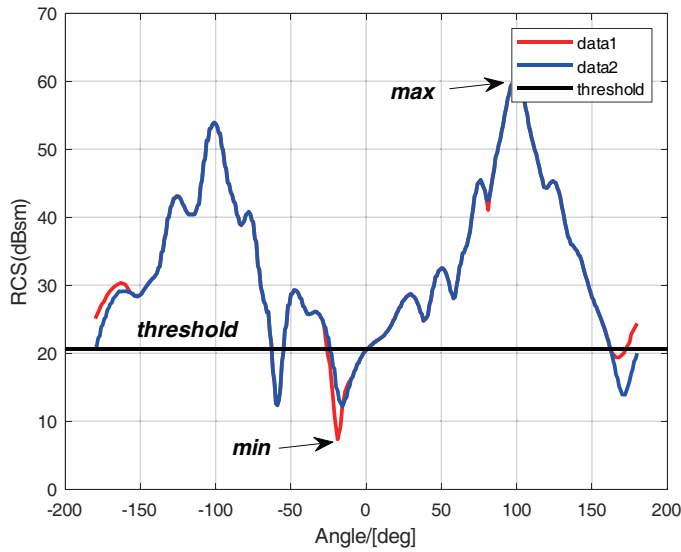


**FIGURE 3.** An example of the RCS Core Area of Interest minimum threshold.

final index of the non-region of interest, because it is impossible to determine whether the credible result of this part is greater or less than the threshold, so the evaluation results here cannot be weakened.

4. The two sets of data are transformed by SPWVD and normalized: taking  $Data_1$  as an example, the transformation process is shown in Eq. (21).

$$W_{Data_1}^{SP}(nk) = \sum_{m=-N}^{m=N} g(n)h(k)z\left(n + \frac{m}{2}\right) * z^*\left(n - \frac{m}{2}\right) e^{-j2\pi km/N} \quad (23)$$

where  $W_{Data_1}^{SP}(nk)$  is the time-frequency energy distribution obtained after SPWVD transformation;  $n$  is the number of points on the horizontal axis of the time-frequency energy distribution map obtained after SPWVD transformation, representing the time domain points, and  $n$  is taken as the length of the data, that is, length ( $Data_1$ );  $k$  is the number of longitudinal axis points of the time-frequency energy distribution map obtained after SPWVD transformation, representing the frequency domain points, and  $k$  is also taken as the data length;  $g(n)$  is a window function that suppresses the intersection of time domain directions, with a length of  $\frac{1}{5}$  of the data length and a Kaiser window with a shape factor of 20 [18];  $h(k)$  is the window function that suppresses the intersection term in the frequency domain; the length is  $\frac{1}{4}$  of the data length, and the Kaiser window with the shape factor is 20. In the same way,  $W_{Data_2}^{SP}(nk)$  can be obtained, and after the transformation is completed,  $W_{Data_1}^{SP}(nk)$  and  $W_{Data_2}^{SP}(nk)$  need to be normalized to prevent the influence of the original data magnitude on the evaluation results. Taking  $Data_1$  as an example, the normalization process is described in Eqs. (22) and (23).

$$W_{Data_{1norm}}^{SP}(nk) = \frac{W_{Data_1}^{SP}(n, k)}{\beta} \quad (24)$$

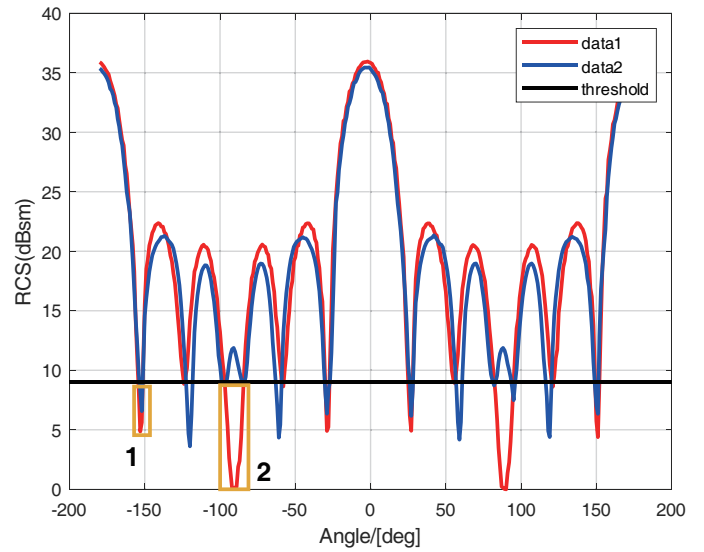


**FIGURE 4.** Legend of non-core area of interest index determination.

$$\beta = \frac{1}{n * k} \left( \sum_{m=1}^{m=n} \sum_{p=1}^{p=k} |W_{Data_1}^{SP}(m, p)| + \sum_{m=1}^{m=n} \sum_{p=1}^{p=k} |W_{Data_2}^{SP}(m, p)| \right) \quad (25)$$

The same goes for  $W_{Data_{2norm}}^{SP}(n, k)$ .

5. Determine the index of frequency points with no energy distribution in the frequency dimension: In the SPWVD transformation, the number of points in the frequency domain is specified as the length of the data, but the energy distribution of the data in the frequency domain may not include all the frequency domain points, so the influence of the frequency domain points without energy distribution on the frequency domain evaluation results should be eliminated. Through the observation of  $W_{Data_{1norm}}^{SP}(nk)W_{Data_{2norm}}^{SP}(nk)$  in the frequency domain, it can be found that there are some frequency points where the energy distribution is very little. In fact, these points have no energy distribution, but the Kaiser window function is used for the SPWVD transformation, so a weak energy distribution is generated, which we can still treat as no energy distribution. In this case, the index needs to be extracted to prepare for the subsequent frequency domain evaluation, as shown in Equations (24), (25).

$$k_{index} = k |_{W_{Data_{1norm}}^{SP}(k) \leq 0.01 * \max(W_{Data_{1norm}}^{SP}(k))} \cap k |_{W_{Data_{2norm}}^{SP}(k) \leq 0.01 * \max(W_{Data_{1norm}}^{SP}(k))} \quad (26)$$

$$W_{Data_{1,2norm}}^{SP}(k) = \sum_{m=1}^{m=n} W_{Data_{1,2norm}}^{SP}(n, k) \quad (27)$$

where  $k_{index}$  is the index of the final frequency domain point with no energy distribution;  $k |_{W_{Data_{1norm}}^{SP}(k)}$  is the index of the

frequency domain point where  $Data_1$  transforms the frequency domain point without energy distribution; and  $k|_{W_{Data_2norm}^{SP}(k)}$

represents the index of the frequency domain point where  $Data_1$  transforms without energy distribution. The reason for the intersection is that if  $Data_1$  has energy distribution at the frequency  $k = p$ , and  $Data_2$  has no energy distribution at the frequency  $k = p$ , it means that there is a difference between the two sets of data at the frequency point, and the difference needs to be retained for frequency domain evaluation.

6. Make a difference between  $W_{Data_1norm}^{SP}(nk)$

and  $W_{Data_2norm}^{SP}(nk)$ : normalize the matrix where

$W_{Data_1norm}^{SP}(nk)$  and  $W_{Data_2norm}^{SP}(nk)$  are both  $n \times k$ , and the difference between the two sets of data is obtained by Equation (26).

$$W_{diff}^{SP}(nk) = ||W_{Data_1norm}^{SP}(nk) - W_{Data_2norm}^{SP}(nk)|| \quad (28)$$

7. Find the average value of each column in the time domain and frequency domain dimensions: the matrix with a difference of  $W_{diff}^{SP}(nk)$  and still  $n \times k$ . The next step is to average it in the time domain and frequency domain

$$W_{diffTmean}^{SP}(n) = \frac{\sum_{p=1}^{p=k} W_{diff}^{SP}(n, k)}{k} \quad (29)$$

$$W_{diffFmean}^{SP}(k) = \frac{\sum_{m=1}^{m=n} W_{diff}^{SP}(n, k)}{n} \quad (30)$$

where  $W_{diffTmean}^{SP}(n)$  is the average value in the time domain

direction, and  $W_{diffFmean}^{SP}(k)$  is the average value in the frequency domain direction.

8. Using the  $x_{index}$  of the points of the non-core area of interest,  $W_{diffTmean}^{SP}(n)$  is divided into two parts,

$$W_{diffTmean}^{SPcore}(n)|_{n \neq x_{index}} \quad \text{and} \quad W_{diffTmean}^{SPNon-core}(n)|_{n = x_{index}}.$$

$W_{diffTmean}^{SPcore}(n)$  represents the time-frequency energy dis-

tribution of the core area of interest, and  $W_{diffTmean}^{SPNon-core}(n)$  represents the time-frequency energy distribution of the non-core area of concern. Use the  $k_{index}$  to remove the frequency point with no energy distribution in  $W_{diffFmean}^{SP}(k)$  to obtain

$W_{diffFmean}^{SPenergy}(k)$  with energy distribution.

9. Time Difference Measure (TDM) and Frequency Difference Measure (FDM) were obtained by classification evaluation of six boxes:  $W_{diffTmean}^{SPcore}(n)$ ,  $W_{diffTmean}^{SPNon-core}(n)$ ,

and  $W_{diffFmean}^{SPenergy}(k)$  were evaluated according to Table 4,  $TDM_{core}(n)$ : the time-domain difference of the core area of interest,  $TDM_{Non-core}(n)$ : the time-domain difference of the non-core area of interest, and  $FDM(k)$ : the frequency-domain difference of the energy distribution region can be obtained.

10. Finally, find the value of the global difference.

$$GDM_c = \sqrt{\left( \begin{array}{c} 0.75 * TDM_{core}^{value} + \\ 0.25 * TDM_{Non-core}^{value} \end{array} \right)^2 + \left( FDM_{energy}^{value} \right)^2} \quad (31)$$

$$TDM_{core}^{value} = \frac{\sum_{i=1}^6 C_{Typical}(i) * TDM_{core}(n)|_{n \neq x_{index}}}{n_{core}} \quad (32)$$

$$TDM_{Non-core}^{value} = \frac{\sum_{i=1}^6 C_{Typical}(i) * TDM_{Non-core}(n)|_{n = x_{index}}}{n_{Non-core}} \quad (33)$$

$$FDM_{energy}^{value} = \frac{\sum_{i=1}^6 C_{Typical}(i) * FDM(k)|_{k \neq k_{index}}}{k_{energy}} \quad (34)$$

#### 4. INSTANCE VERIFICATION

Take  $Data(a)$  as an example.

1. The index for the non-core region of interest is  $[(-61, -54), (-23, 1), (164, 173)]$  from Figure 5.

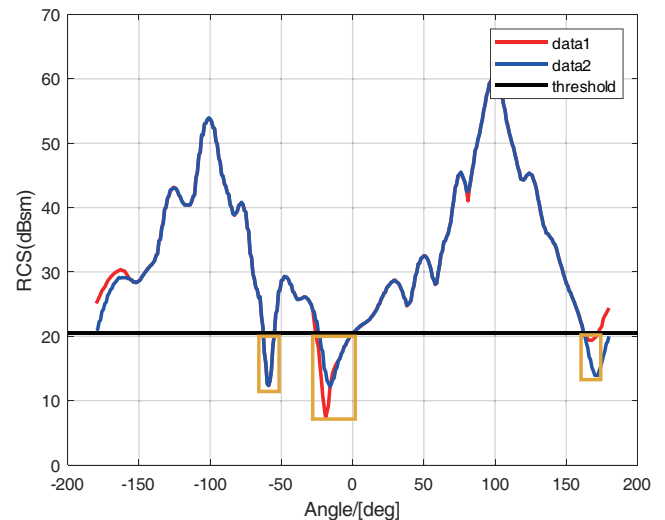


FIGURE 5. An example of a time domain index.

2. After SPWVD transformation and normalization processing, the normalized time-frequency distribution of the two sets of data can be obtained, as shown in Figures 6 and 7.

3. The index for the energy distribution region is  $[(1-55), (336-360)]$  from Figure 8.

4. Making a difference between the two matrices obtained in step 2 yields Figure 9.

5. The matrices obtained in step 4 are averaged along the time and frequency domains, respectively, to obtain Figures 10 and 11.

6. Figures 12-14 can be obtained by combining the time-domain index and frequency-domain index to classify the two plots in step 5 by performing a six-box evaluation classification.

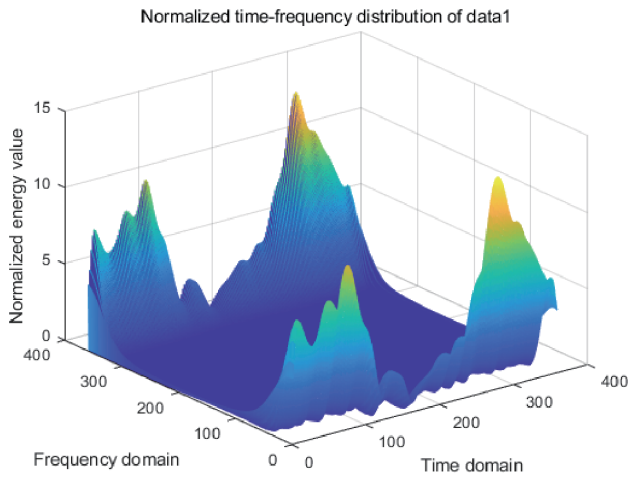


FIGURE 6. Data 1 normalized time-frequency distribution.

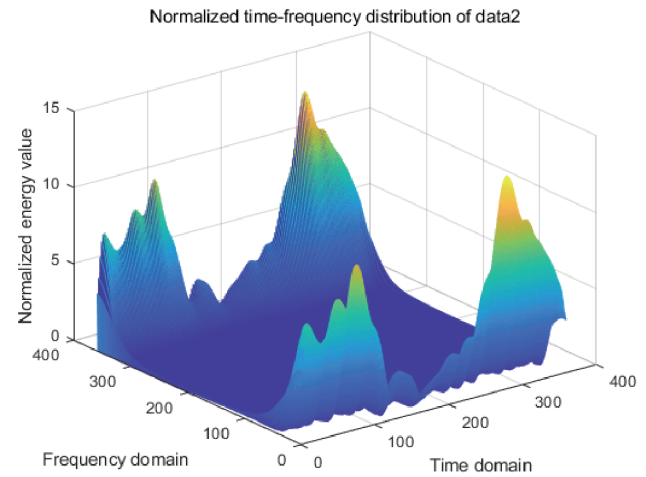


FIGURE 7. Data 2 normalized time-frequency distribution.

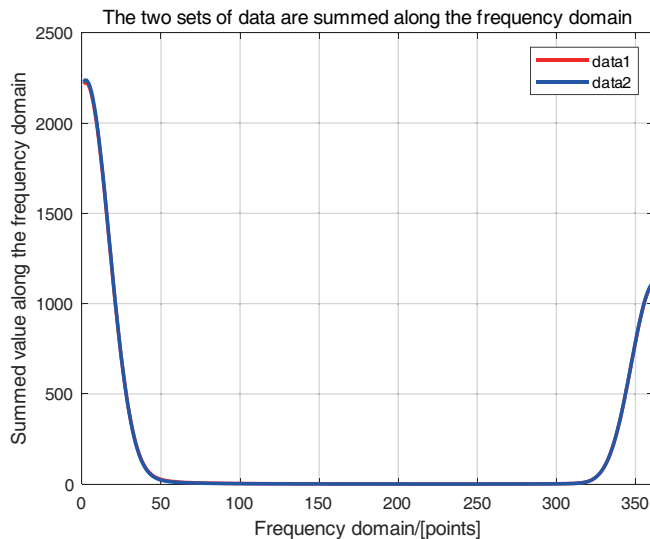


FIGURE 8. An example of a frequency domain index.

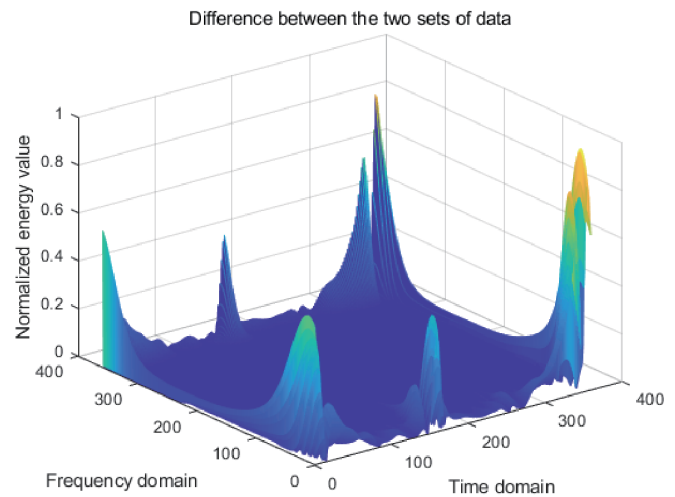


FIGURE 9. The difference between the two matrices.

7. Using the classification results in step 6, combined with the weight assignment and Equations (29)–(32), the value of the global difference is calculated. Take data A) as an example, the calculation process is as follows:

$$TDM_{core}^{value} = \frac{[1, 2, 3, 4, 5, 6] * [103, 196, 9, 6, 2, 1]}{317} = 1.7728 \quad (35)$$

$$TDM_{Non-core}^{value} = \frac{[1, 2, 3, 4, 5, 6] * [8, 29, 6, 0, 0, 0]}{43} = 1.9534 \quad (36)$$

$$FDM_{energy}^{value} = \frac{[1, 2, 3, 4, 5, 6] * [0, 44, 17, 19, 0, 0]}{80} = 2.6875 \quad (37)$$

$$GDM_c = \sqrt{(0.75 * 1.7728 + 0.25 * 1.9534)^2 + (2.6875)^2}$$

$$= 3.2447 \quad (38)$$

The above processing is carried out on all 8 sets of data in Figure 1, and a set of data [3.24, 4.82, 4.98, 6.23, 5.16, 6.64, 5.56, 4.59] can be obtained.

In the SPWVD algorithm,  $y_{threshold}$  is used to divide the core area of interest, so the results obtained by directly using the FSV algorithm on the data cannot be compared with the results obtained using the SPWVD algorithm, because the data sets used are essentially different, so we need to perform the operations described in steps 1–3 of Subsection 3.2 on the initial data before using the FSV algorithm.

The results shown in Table 5 and Table 6 can be obtained by using the above algorithm and then using Eqs. (15), (16) to standardize the evaluation values of the algorithm.

According to the above table, compared with using FSV directly on the data, FSV on the preprocessed data is more consistent with the expert evaluation only at the data d), which may be related to the selection of thresholds. The effect may be better

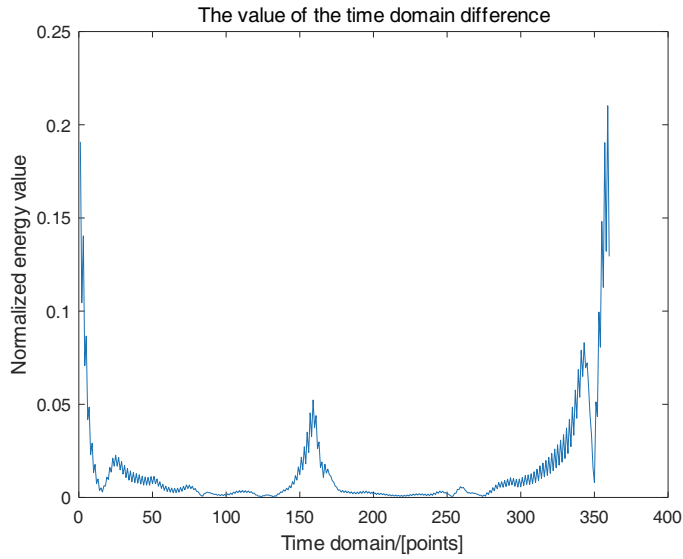


**FIGURE 10.** The matrices obtained in step 4 is averaged along the time domain.

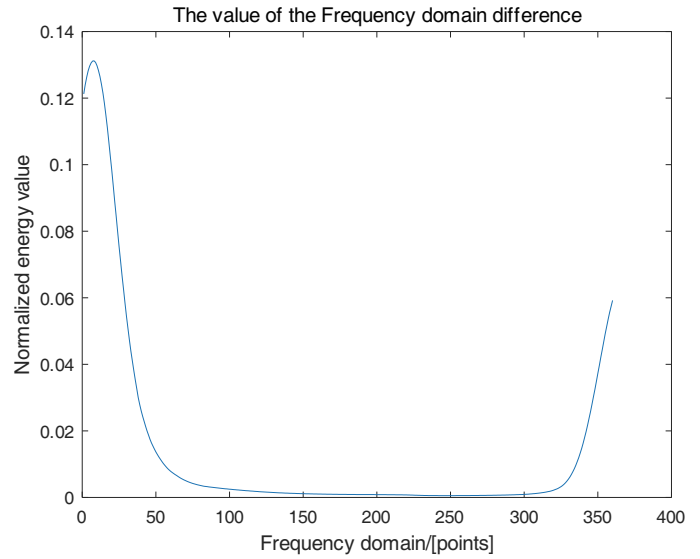


**FIGURE 11.** The matrices obtained in step 4 is averaged along the frequency domain.

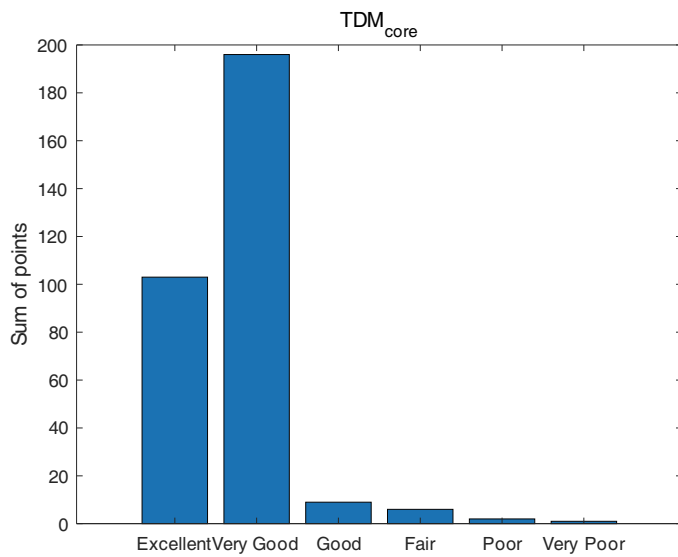


**FIGURE 12.** The time-domain core area of interest is classified into 6 boxes.

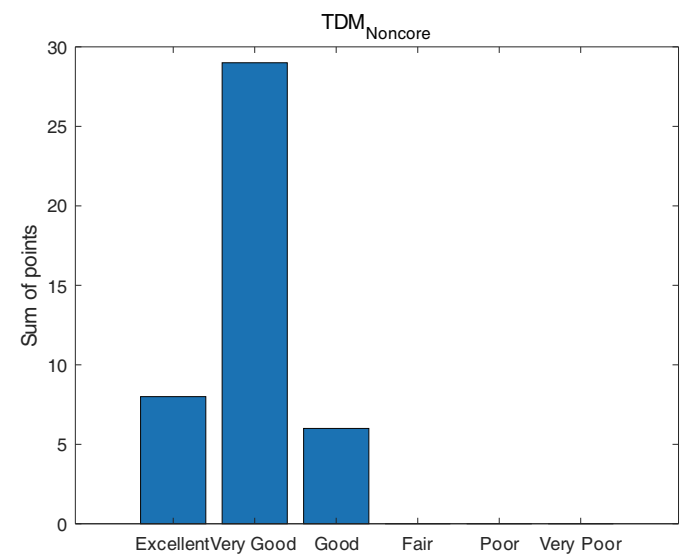


**FIGURE 13.** The time-domain Non-core area of interest is classified into 6 boxes.

**TABLE 5.** Standardized evaluation results and comparison of different evaluation methods.

	Expert survey results	FSV results	FSV on Weighted data results	SPWVD-ON-RCS results
Data1	0	0	0	0
Data 2	0.4775	0.1407	0.2810	0.4647
Data 3	0.5020	0.5885	0.6409	0.5118
Data 4	0.6148	0.8213	0.6222	0.8794
Data 5	0.5902	0.4553	0.5098	0.5647
Data 6	1.0000	1.0000	1.0000	1.0000
Data 7	0.6373	0.7405	0.6000	0.6824
Data 8	0.4098	0.5095	0.6052	0.3971

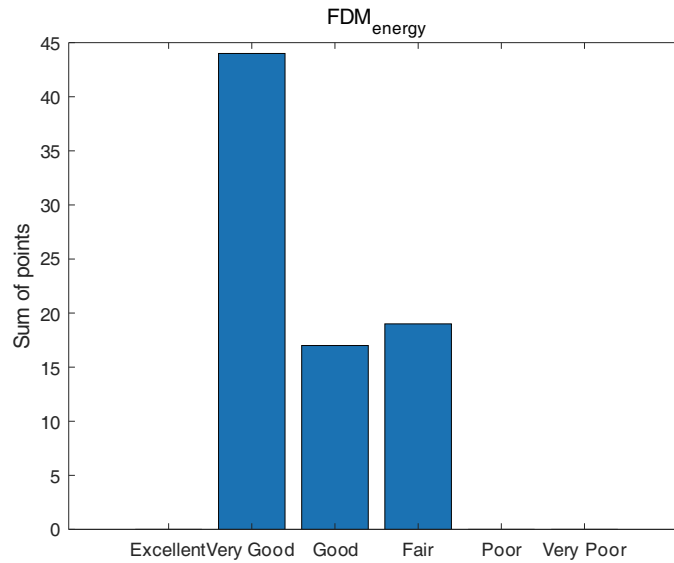


FIGURE 14. The frequency-domain energy area is classified into 6 boxes.

TABLE 6. Standardized evaluation results sorting and comparison of different evaluation methods.

	Expert survey sorting	FSV sorting	FSV on Weighted data sorting	SPWVD-ON-RCS sorting
Data 1	1	1	1	1
Data 2	3	2	2	3
Data 3	4	5	7	4
Data 4	6	7	6	7
Data 5	5	3	3	5
Data 6	8	8	8	8
Data 7	7	6	4	6
Data 8	2	4	5	2

if a threshold that is more suitable for the FSV algorithm can be chosen. The algorithm proposed in this paper is basically consistent with the expert evaluation in the RCS data, but there are also some errors. For example, in Data d), the error of the two results reaches 0.2646, while the error of the other 7 sets of data is less than 0.05. The reason is that when evaluating Data d), experts agree that the overall consistency of the data in terms of trend and characteristics has a certain tolerance for the magnitude of the data, but the algorithm equally evaluates the magnitude, trend, characteristics, and other indicators of the data, so the evaluation error is generated.

## 5. CONCLUSION

Data verification technology is an effective method to improve the reliability and practicability of RCS data, which is of great significance for measurement and simulation optimization in radar-related fields. In this paper, the limitations of the FSV method applied to RCS data are analyzed through the investigation of experts in the field of radar, and a new method is proposed. The validation results of 8 sets of typical RCS data show that the evaluation results of RCS data proposed in this paper are obviously close to the results of expert evaluation and have strong applicability.

## ACKNOWLEDGEMENT

This work is sponsored by the National Nature Science Foundation of China (62231007) and the National Key Laboratory of Air-based Information Perception and Fusion and the Aeronautical Science Foundation(20230001077006).

## REFERENCES

- [1] Liu, Y. and X. Zhao, "Perfect absorber metamaterial for designing low-RCS patch antenna," *IEEE Antennas and Wireless Propagation Letters*, Vol. 13, 1473–1476, 2014.
- [2] "IEEE standard for validation of computational electromagnetics computer modeling and simulations," *IEEE Std 1597.1-2022 (Revision of IEEE Std 1597.1-2008)*.
- [3] Lash, P. C., "Comparison of computational electromagnetic codes for prediction of low-frequency radar cross section," Master thesis, Air Force Institute of Technology, Wright-Patterson AFB, OH, USA, 2006.
- [4] Zhou, B., H. Dai, Y. Zhang, and H. Qiao, "Validation of maneuvering target RCS by computation based on feature selective validation (FSV)," in *2018 Cross Strait Quad-Regional Radio Science and Wireless Technology Conference (CSQRWC)*, 1–2, Xuzhou, China, 2018.
- [5] Johnson, M. R. and E. L. Coffey, "Using FSV with far-field patterns," in *2012 IEEE International Symposium on Electromag-*

- netic Compatibility, 696–701, Pittsburgh, PA, USA, 2012.
- [6] Drozd, A., I. Kasperovich, J. Norgard, and R. Musselman, “Feature Selected Validation and verification (FSVV) of CEM code predictions using IR thermal images of EM fields,” in *2008 Asia-Pacific Symposium on Electromagnetic Compatibility and 19th International Zurich Symposium on Electromagnetic Compatibility*, 359–362, Singapore, 2008.
- [7] Zhang, G., A. P. Duffy, H. Sasse, L. Wang, and R. Jauregui, “Improvement in the definition of ODM for FSV,” *IEEE Transactions on Electromagnetic Compatibility*, Vol. 55, No. 4, 773–779, Aug. 2013.
- [8] Duffy, A. P., A. J. M. Martin, A. Orlandi, G. Antonini, T. M. Benson, and M. S. Woolfson, “Feature selective validation (FSV) for validation of computational electromagnetics (CEM). part I-the FSV method,” *IEEE Transactions on Electromagnetic Compatibility*, Vol. 48, No. 3, 449–459, Aug. 2006.
- [9] Martin, W. and P. Flandrin, “Wigner-Ville spectral analysis of nonstationary processes,” *IEEE Transactions on Acoustics, Speech, and Signal Processing*, Vol. 33, No. 6, 1461–1470, Dec. 1985.
- [10] Martin, A. J. M., “Quantitative Data Validation,” Ph.D. dissertation, De Montfort University, Leicester, UK, 1999.
- [11] Jauregui, R., G. Zhang, J. Rojas-Mora, O. Ventosa, F. Silva, A. P. Duffy, and H. Sasse, “Analyzing transient phenomena in the time domain using the feature selective validation (FSV) method,” *IEEE Transactions on Electromagnetic Compatibility*, Vol. 56, No. 4, 825–834, Aug. 2014.
- [12] “IEEE standard for validation of computational electromagnetics computer modeling and simulations,” IEEE Std 1597.1-2008, 1–36, May 2009.
- [13] Welch, P., “The use of fast Fourier transform for the estimation of power spectra: A method based on time averaging over short, modified periodograms,” *IEEE Transactions on Audio and Electroacoustics*, Vol. 15, No. 2, 70–73, Jun. 1967.
- [14] Donoho, D. L., “Compressed sensing,” *IEEE Transactions on Information Theory*, Vol. 52, No. 4, 1289–1306, Apr. 2006.
- [15] Khare, S. K. and V. Bajaj, “Time-frequency representation and convolutional neural network-based emotion recognition,” *IEEE Transactions on Neural Networks and Learning Systems*, Vol. 32, No. 7, 2901–2909, Jul. 2021.
- [16] Zhang, Z., C. Wang, C. Gan, S. Sun, and M. Wang, “Automatic modulation classification using convolutional neural network with features fusion of SPWVD and BJD,” *IEEE Transactions on Signal and Information Processing over Networks*, Vol. 5, No. 3, 469–478, Sep. 2019.
- [17] Kalra, M., S. Kumar, and B. Das, “Moving ground target detection with seismic signal using smooth pseudo Wigner-Ville distribution,” *IEEE Transactions on Instrumentation and Measurement*, Vol. 69, No. 6, 3896–3906, Jun. 2020.
- [18] Putranto, P., W. Desvasari, P. Daud, Y. N. Wijayanto, D. Mahmudin, D. P. Kurniadi, A. N. Rahman, S. Hardiati, A. Setiawan, F. Darwis, *et al.*, “Performance comparison of Blackman, Bartlett, Hanning, and Kaiser window for radar digital signal processing,” in *2019 4th International Conference on Information Technology, Information Systems and Electrical Engineering (ICITISEE)*, 391–394, Yogyakarta, Indonesia, 2019.